MDPI

Article

Effects of Roughness on Stresses in an Oxide Scale Formed on a Superalloy Substrate

Yang Zhao [1,2,*], Fan Sun [3], Peng Jiang [3,*] and Yongle Sun [4]

1   CAS Key Laboratory of Human-Machine Intelligence-Synergy Systems, Shenzhen Institutes of Advanced Technology, Chinese Academy of Sciences, Shenzhen 518055, China

2   Department of Materials, School of Natural Sciences, University of Manchester, Manchester M13 9PL, UK

3   State Key Laboratory for Strength and Vibration of Mechanical Structures, School of Aerospace Engineering, Xi'an Jiaotong University, Xi'an 710049, China; sf2038945624@163.com

4   Welding Engineering and Laser Processing Centre, School of Aerospace, Transport and Manufacturing, Cranfield University, Cranfield MK43 0AL, UK; yongle.sun@cranfield.ac.uk

*   Correspondence: yang.zhao@siat.ac.cn (Y.Z.); jiangpeng219@mail.xjtu.edu.cn (P.J.)

Abstract: The effects of surface roughness on the stresses in an alumina scale formed on a Fecralloy substrate are investigated. Spherical indenters were used to create indents with different radii and depths to represent surface roughness and then the roughness effect was studied comprehensively. It was found that the residual stresses in the alumina scale formed around the rough surface are almost constant and they are dominated by the curvature rather than the depth of the roughness. Oxidation changes the surface roughness. The edge of the indent was sharpened after oxidation and the residual stress there was released presumably due to cracking. The residual stresses in the alumina scale decrease with increase in oxidation time, while the substrate thickness has little effect, given that the substrate is thicker than the alumina scale. Furthermore, the effect of roughness on the oxide growth stress is analysed. This work indicates that the surface roughness should be considered for evaluation of stresses in coatings.

1. Introduction

During oxidation of high temperature alloys, e.g., Ni based superalloy and FeCrAl alloy, the stress in the oxide scale formed on the substrate plays an important role in spallation of the oxide scale. Thermally grown oxide (TGO), mostly alumina, forms in thermal barrier coatings (TBCs), when TBCs are exposed to high temperature environment; and spallation of TGO leads to failure of TBCs [1–8]. It is generally agreed that the stress in TGO varies with the undulating morphology of the oxide scale [9]. Some finite element models were employed to investigate the effect of TGO geometry on stresses [10,11]. Ranjbar-Far et al. [10] studied the effect of the undulation amplitudes at interfaces and found that the maximum value of tensile stress at semi-circular interface was higher than that of the sinusoidal interface. Considering that the TGO thickness is not uniform, finite element models of geometrically heterogeneous TGO were developed for analysis [12,13], revealing that the TGO in the apex areas of the undulation was thicker than that in the valley areas, and nonuniform TGO was more likely to induce TBCs spallation. Song et al. [14] established a TGO growth model with different growth rates at different locations. They demonstrated that the nonuniform growth of TGO would lead to increase of residual stresses at flank locations, as well as early interfacial cracks. Thus, the morphology of TGO has important effects on the stress level. Previous research has also shown that the rumpling of the TGO layer (i.e., roughness of TGO varies) during thermal cycling could cause the failure of TBCs [1,15–18]. In general, the standard deviation of the height of surface, R_q, is used as the roughness parameter. However, TBCs with similar TGO roughness, R_q,

can exhibit different lifetime before coatings spallation, which has not received enough attention and research.

To evaluate the influence of TGO roughness on TBCs lifespan, the stresses of TGO with different roughness parameters need to be determined. Previous research has used several types of experimental techniques to obtain the stresses in TBCs, i.e., nano-indentation, X-ray diffraction (XRD), Raman spectroscopy and photoluminescence piezo-spectroscopy (PLPS). Based on the relationship between the Young's modulus measured by nano-indentation and the stress in the material, the residual stresses in TBCs were obtained [19,20]. However, the nano-indentation method is only applicable to the measurement of surface stress. The XRD and Raman spectroscopy have been widely used in the non-destructive stress measurement, but they are not suitable to obtain the TGO stress in TBCs due to their limitation of penetration depth [21,22]. By contrast, based on the relationship between stress and peak shift of Cr^{3+} luminescence, PLPS can penetrate through the ceramic top coat, and has been used as a very powerful and relatively accurate method in the TGO stress measurement [7,23,24]. Therefore, the PLPS method is used in this work to measure the change of the TGO stress affected by surface roughness.

In this study, the effects of surface roughness on the stresses in an alumina scale formed on a Fecralloy substrate are investigated. spherical indenters are used to produce indents (i.e., roughness of surface) with different radii and depths before formation of TGO on a Fecralloy substrate. The effects of radius and depth on TGO stresses for different periods of oxidation are measured through PLPS method and then analysed in detail.

2. Experiments

Fecralloy (Fe72.8Cr22Al5Y0.1Zr0.1 in wt. %, Goodfellow, UK) was used for the present study as it could form a uniform and adherent α-Al_2O_3 scale. Button-like substrates, of diameter of 25.4 mm, were cut and then mechanically polished to a 0.25 μm finish on both sides and cleaned in acetone. Three spherical indenters with radii of 20, 200 and 1000 μm were employed with various levels of loading to create roughness on the polished samples with different radii and depths. The 20 μm and 200 μm radii indents were generated by instrumented micro-indentation, while the 1000 μm one was created by Rockwell tester. One group of the samples with the same thickness of approximate 2 mm were oxidised in ambient air at 1200 °C for 1, 4, 9 and 16 h. The other groups consisting of the samples with thickness of 1, 2, 3 and 4 mm were oxidised at 1200 °C for 25 h. After oxidation, all samples were taken from the furnace immediately and cooled by air blasting to prevent plastic relaxation of the substrate. The profiles of indents were measured by interferometer (MicroXAM, KLA-Tencor, Milpitas, CA, USA) prior to and after oxidation. The residual stress in the alumina scale was measured at room temperature using PLPS (HR 800, Horiba, Paris, France) and 532-nm laser with an optimal probe size of about 3 μm, where the peak shift of spectra was used to determine the residual stress. Several samples were additionally cooled in liquid nitrogen. The experimental steps were shown in Figure 1. The stresses in these samples were measured and compared to the values from air cooling samples. The results showed identical measured stress value and, therefore, it was reasonable to assume that no considerable plastic relaxation occurred during cooling.
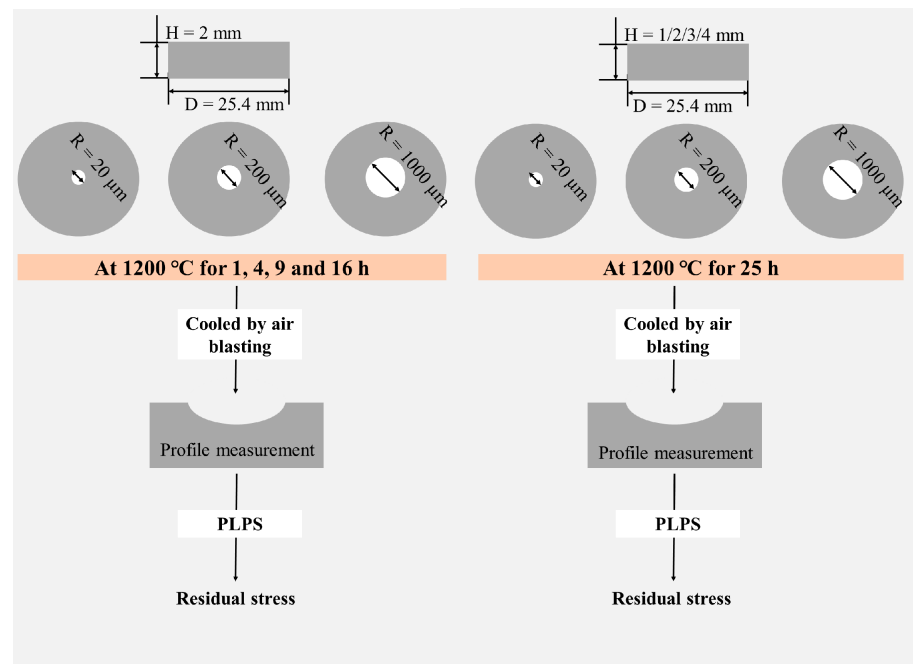
Figure 1. Experimental process diagram.

3. Results and Discussion

Figure 2 shows the profiles of one typical indent before and after oxidation. Significant spikes are present at the edge of the indent after oxidation. The depth, *h*, and the span, *l*, of a typical indent are listed in Table 1. The radius of the indent can be obtained according to $R = \left\{ h^2 + (l/2)^2 \right\}/2h$. The calculated radius is 203 μm and the radius of the spherical indenter is 200 μm. Hence the radii obtained from the indents before oxidation agree very well with the geometry of spherical indenters, but deviation occurred after oxidation, because the depths of indents increased after oxidation (Table 1), which indicated that the oxide scale formed was generally thicker at the flat surface than at indents. This also agrees with previous study by Tolpygo and Clarke [9].

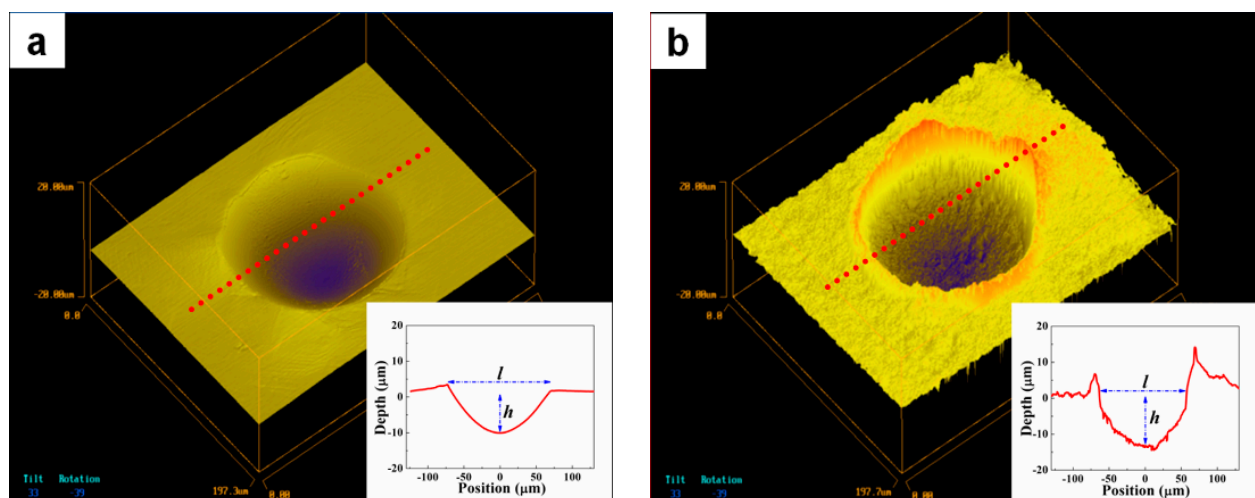**Figure 2.** The profiles of a typical indent created by a spherical indenter with 200 μm radius using 30 N loading prior to (**a**) and after (**b**) oxidation at 1200 °C for 25 h. The inset is the line scan of the location indicated by the red dotted line.

Table 1. The depth, span and calculated radius of a typical indent shown in Figure 1.

Conditions	h (µm)	l (µm)	R (µm)
Before oxidation	10 ± 2	126 ± 3	203 ± 4
After oxidation	13 ± 3	120 ± 6	145 ± 7

Figure 3 shows a typical profile of the peak shift across an indent. The peak shift is nearly constant at the flat surface and decreases to almost zero at the edge of the indent, and then increases to a constant value across most of the central part of the indent. Significant decohesion of TGO from substrate is inferred to occur at the edge of the indents, hence leading to zero stress in the TGO. The following study will focus on the peak shift of TGO at the central part of indents.
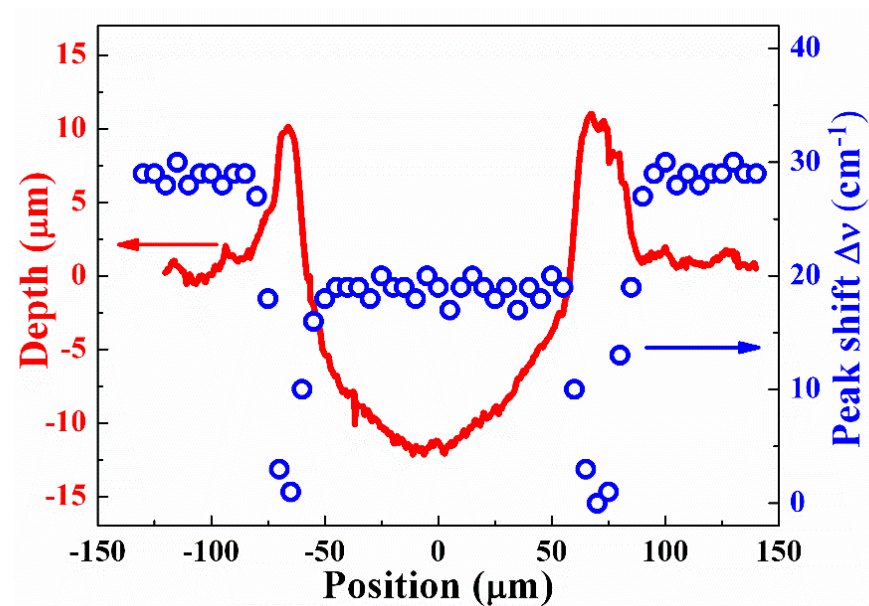
Figure 3. A typical profile of the peak shift of the characteristic R-line of α-Al$_2$O$_3$ scale across the indent created by a 200 µm radius indenter with 30 N loading after oxidation at 1200 °C for 25 h.

The stress can be derived from the peak shift ($\Delta\nu$) of the characteristic R-lines of the Cr^{3+} luminescence relative to the stress-free alumina given by [25,26]:

$$\Delta\nu = \frac{1}{3}\Pi_{ii}\sigma_{ii} \tag{1}$$

where σ_{ii} are the hydrostatic components of the stress tensor and Π_{ii} are the components of the piezospectroscopic tensor ($\Pi_{ii} = 7.60$ cm^{-1}/GPa for α-Al$_2$O$_3$) [26]. For a flat scale, the stress can be assumed to be biaxial, i.e., $\sigma_{xx} = \sigma_{yy} = \sigma$ and $\sigma_{zz} = 0$. Therefore, the biaxial stress can be determined by $\Delta\nu = 5.06\,\sigma$. However, for a curved alumina scale, the component σ_{zz} normal to the sample surface is no longer zero and the in-plane stress components σ_{xx} and σ_{yy} are expected to vary from place to place, depending on the geometry of oxide. For a spherically symmetric geometry like the spherical indent in this study, an analytical solution for the thermal mismatch stress is obtained as [27]:

$$\sigma_{zz} = \frac{E_{ox}(\alpha_{sub} - \alpha_{ox})\Delta T\left[1 - \left(\frac{R-H}{R}\right)^3\right]}{1 - 2\nu_{ox} + \frac{1+\nu_{ox}}{2}\left(\frac{R-H}{R}\right)^3 + \frac{E_{ox}}{E_{sub}}\left(\frac{1+\nu_{sub}}{2}\right)\left[1 - \left(\frac{R-H}{R}\right)^3\right]} \tag{2}$$

$$\sigma_{xx} = \sigma_{yy} = \frac{\left[1 + \frac{1}{2}\left(\frac{R-H}{R}\right)^3\right]}{\left[1 - \left(\frac{R-H}{R}\right)^3\right]}\sigma_{zz} \tag{3}$$

where the oxide scale and the substrate are distinguished by subscripts "sub" and "ox", respectively, H is the oxide thickness, R is the radius of the indent, α is the thermal expansion coefficient, E is Young's modulus, ν is Poisson's ratio and ΔT is the temperature change. The indents created by spherical indenters in this study are close to spherical geometry, so the equations are used to estimate the stresses. From Equations (1)–(3), the peak shift induced by thermal mismatch stress can be calculated.

PLPS measurements below were made on the alumina scale formed at the central part of indents with various radii and depths. Figure 4a summarises the peak shift as a function of indent radius and depth after oxidation at 1200 °C for 25 h. As the radius of indent (or the reciprocal of curvature) increases, the peak shift, i.e., stress increases. In the case of 1000 μm radius which has a very small curvature, the determined value is almost the same as that of a flat surface. According to Equations (2) and (3), normalised tangential stress σ_{xx}, σ_{yy} and normal stress σ_{zz} as a function of the indent radius and oxide thickness ratio are shown in Figure 4b, where σ_0 is the stress at a flat surface, $\sigma_0 = \frac{E_{ox}\Delta\alpha\Delta T}{1-\nu_{OX}}$. The σ_{zz} decreases but σ_{xx} increases with increasing radius. Since $\Delta\nu = \frac{1}{3}\Pi_{ii}(\sigma_{xx} + \sigma_{yy} + \sigma_{zz})$, the peak shift follows the same trend as the tangential stress, hence, it increases with an increase in the radius. According to Figure 4a, the indent depth has no obvious effect on the peak shift, as also shown in Equations (2) and (3). Such conclusion is striking, considering the practical cases in the application field such as TBCs where standard deviation of the depth of roughness is usually used as the parameter to quantify the rumpling effect of TGO interface which is believed to be one of mechanisms accounting for the ultimate failure of TBCs.
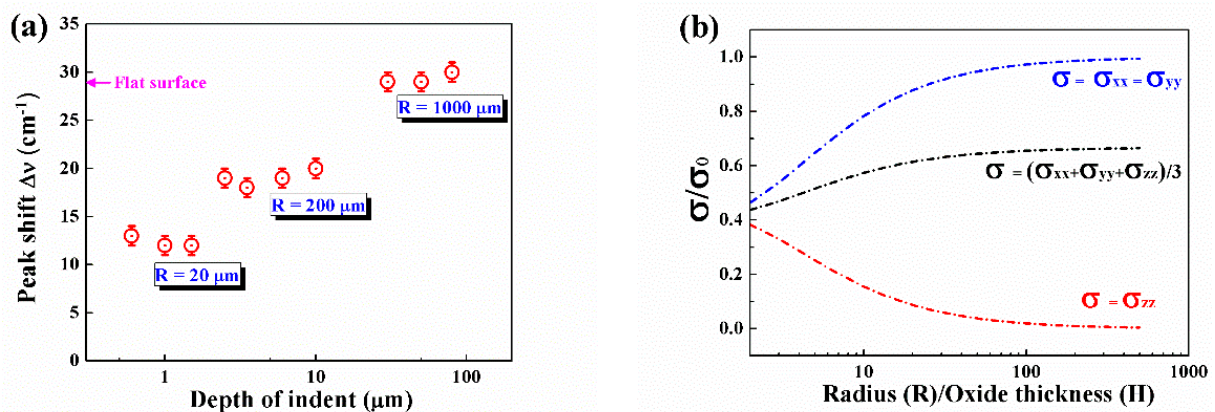

Figure 4. (**a**) Peak shift of the characteristic R-line of α-Al$_2$O$_3$ scale formed at the central part of the indents on Fecralloy after oxidation at 1200 °C for 25 h as a function of indent radius and depth. (**b**) Normalised σ_{zz} and σ_{xx} (σ_{yy}) as a function of the indent radius and oxide thickness ratio, R/H.

Figure 5a reveals the peak shift from measurements at indents as a function of oxidation time and substrate thickness. The peak shift decreases as the oxidation time increases. During oxidation the oxide scale thickens, and according to Figure 4b, the total stress which is defined as the arithmetic mean of axial stress components decreases with increasing oxide thickness, given the same radius of indent, hence, the peak shift declines with the oxidation time. In addition, the substrate thickness has no obvious effect on the peak shift because the substrate is much thicker than the oxide scale in the study and it does not have plastic deformation during cooling, and also according to Equations (1)–(3) the substrate thickness is not included in the stress prediction, given that the substrate is significantly

thicker than the alumina scale, therefore the peak shifts on the substrates of different thickness led to similar values.
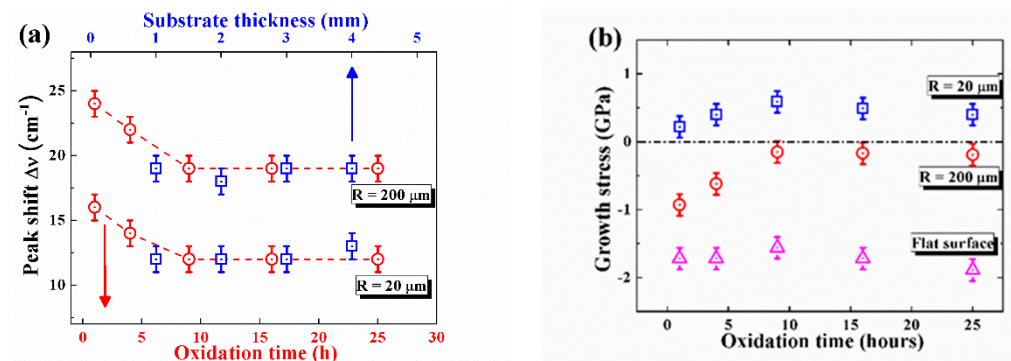

Figure 5. (**a**) Peak shift of the characteristic R-line of α-Al$_2$O$_3$ scale at the indents with 20 μm and 200 μm radii as a function of oxidation time at 1200 °C with circle symbols (given a substrate thickness of 2 mm) and substrate thickness with square symbols (given an oxidation period of 25 h). (**b**) Calculated growth stress of alumina scale formed on the flat surface and the indents with 20 μm and 200 μm radii as a function of oxidation time at 1200 °C.

It is noted that the peak shift becomes stable gradually after initial decrease with extended oxidation time, where the change in stresses cannot be explained purely based on thermal mismatch stress according to the Equations (1)–(3) in which only thermal mismatch stress has been considered. The residual stress in the oxide scale at room temperature comprises two components, i.e., the thermal mismatch stress and the oxide growth stress. Generally, the mismatch stress is larger than the growth stress, so the changing trend of the total stress based on the peak shift as a function of indent depth and radius can be explained well with Equations (1)–(3). However, in order to understand the effect of oxidation time on the stresses in alumina scale and also conduct a quantitative analysis, the growth stress must be considered, which will be discussed below.

The growth stress, σ$_{growth}$, in the scale at the oxidation temperature can be obtained from the room temperature stress data using the following equation:

$$\Delta \nu = \frac{1}{3} \times 7.60 \times \left(\sigma_{xx} + \sigma_{yy} + \sigma_{zz} + 2 \cdot \frac{E_{sub}}{E_{ox}} \sigma_{growth} \right) \qquad (4)$$

where the thermal expansion coefficients of the substrate and oxide are, α_{sub} =14.0 × 10^{-6}/°C and α_{ox} = 8.2 × 10^{-6}/°C, respectively [28], the Young's moduli of the substrate and oxide are, E_{sub} = 200 GPa and E_{ox} = 400 GPa, respectively, while E_{ox}^T = 330. GPa is the oxide Young's modulus at 1200 °C [28], ΔT is the temperature drop from oxidation temperature (ΔT = 1175 °C). The Poisson's ratio is taken to be ν_{sub} = 0.3 and ν_{ox} = 0.25 for the substrate and oxide, respectively. The oxide thickness H was measured by scanning electron microscope (SEM) images and determined to be 0.7, 1.4, 2.2, 2.9 and 3.6 μm for samples oxidised at 1200 °C for 1, 4, 9, 16 and 25 h, respectively. Using the peak shift data in Figure 4a and Equations (2)–(4), the growth stress can be obtained.

The growth stress of the oxide scale is presented in Figure 5b. The difference between the oxide growth stresses at the indents of different radii is remarkable. For the indent of 20 μm radius, the growth stress is tensile from the beginning of oxidation. On contrary, the growth stress is compressive for the indent of 200 μm radius and it decreases as a function of oxidation time. The compressive growth stress formed on a flat surface rises up to about 1.7 GPa and is almost constant through the oxidation period carried out in the study. The tensile stress within the indent of small radius (large curvature) could be because complicated oxide growth occurred due to the large curvature, and partial stress relaxation might occur in this region during cooling. The analysis above is based on the assumption that there is no plastic deformation of the substrate during temperature change.

It is reasonable for a flat surface or locations with small curvatures because the stress in the substrate is small and relatively uniform. However, the presence of an indent with a very large curvature could lead to a nonuniform stress redistribution in the subscale region of the substrate with relatively high stresses in specific areas [9,27]. In addition, the assumption of the spherical configuration of the indent is not exactly valid for samples after oxidation, as shown in Table 1. These can result in some errors in the data. Despite the limitations in the measurement method, the experimental results indicate that the curvature of roughness has an important effect on the growth stress in the oxide scale.

4. Conclusions

In summary, the effects of the depth and curvature of surface roughness on the stresses in an alumina scale formed on a FeCrAlY substrate are investigated using the photostimulated luminescence piezospectroscopy method. It was found that the roughness curvature, rather than the roughness depth, dominates the residual stress in the alumina scale. Oxidation affects the roughness profile and causes stress relaxation on the edge of the indent, which can be correlated with local cracking. The residual stress in the rough alumina scale decreases with oxidation time increasing, while it is insensitive to the thickness of the substrate which is thicker than the aluminium scale. The complicated variation of oxide growth stress with oxidation time is also revealed. This study demonstrates that the surface roughness should be precisely considered in stress analysis for TGO and TBCs.

Author Contributions: Conceptualization, Y.Z., P.J. and Y.S.; methodology, Y.Z.; software, Y.Z.; validation, P.J. and Y.S.; formal analysis, Y.Z., P.J. and Y.S.; investigation, Y.Z., F.S.; resources, P.J.; data curation, P.J.; writing—original draft preparation, Y.Z., P.J. and F.S.; writing—review and editing, F.S., Y.S.; visualization, Y.Z. and Y.S.; project administration, Y.Z. All authors have read and agreed to the published version of the manuscript.

Institutional Review Board Statement: Not applicable.

Informed Consent Statement: Not applicable.

Data Availability Statement: The data presented in this study are available on request from the corresponding author after obtaining permission of authorized person.

Conflicts of Interest: The authors declare no conflict of interest.

References

1. Evans, A.G.; Mumm, D.R.; Hutchinson, J.W.; Meier, G.H.; Pettit, F.S. Mechanisms controlling the durability of thermal barrier coatings. *Prog. Mater. Sci.* **2001**, *46*, 505–553. [CrossRef]
2. Clarke, D.R.; Levi, C.G. Materials design for the next generation thermal barrier coatings. *Annu. Rev. Mater. Res.* **2003**, *33*, 383–417. [CrossRef]
3. Clarke, D.R.; Christensen, R.J.; Tolpygo, V. The evolution of oxidation stresses in zirconia thermal barrier coated superalloy leading to spalling failure. *Surf. Coat. Technol.* **1997**, *94*, 89–93. [CrossRef]
4. Teixeira, V.; Andritschky, M.; Fischer, W.; Buchkremer, H.P.; Stover, D. Effects of deposition temperature and thermal cycling on residual stress state in zirconia-based thermal barrier coatings. *Surf. Coat. Technol.* **1999**, *120*, 103–111. [CrossRef]
5. Sohn, Y.H.; Kim, J.H.; Jordan, E.H.; Gell, M. Thermal cycling of EB-PVD/MCrAlY thermal barrier coatings: I. Microstructural development and spallation mechanisms. *Surf. Coat. Technol.* **2001**, *146*, 70–78. [CrossRef]
6. Jiang, P.; Yang, L.; Sun, Y.; Li, D.; Wang, T. Nondestructive measurements of residual stress in air plasma-sprayed thermal barrier coatings. *J. Am. Ceram. Soc.* **2020**, 1–10. [CrossRef]
7. Jiang, P.; Fan, X.; Sun, Y.; Wang, H.; Su, L.; Wang, T. Thermal-cycle dependent residual stress within the crack-susceptible zone in thermal barrier coating system. *J. Am. Ceram. Soc.* **2018**, *101*, 4256–4261. [CrossRef]
8. Jiang, J.; Ma, X.; Wang, B. Stress analysis of the thermal barrier coating system near a cooling hole considering the free-edge effect. *Ceram. Int.* **2020**, *46*, 331–342. [CrossRef]

9. Tolpygo, V.K.; Clarke, D.R. Wrinkling of α-alumina films grown by thermal oxidation—I. Quantitative studies on single crystals of Fe–Cr–Al alloy. *Acta Mater.* **1998**, *46*, 5153–5166. [CrossRef]

10. Ranjbar-Far, M.; Absi, J.; Mariaux, G.; Dubois, F. Simulation of the effect of material properties and interface roughness on the stress distribution in thermal barrier coatings using finite element method. *Mater. Des.* **2010**, *31*, 772–781. [CrossRef]

11. Ranjbar-Far, M.; Absi, J.; Mariaux, G. Finite element modeling of the different failure mechanisms of a plasma sprayed thermal barrier coatings system. *J. Therm. Spray Technol.* **2012**, *21*, 1234–1244. [CrossRef]

12. Chen, Z.; Huang, H.; Zhao, K.; Jia, W.; Fang, L. Influence of inhomogeneous thermally grown oxide thickness on residual stress distribution in thermal barrier coating system. *Ceram. Int.* **2018**, *44*, 16937–16946. [CrossRef]

13. Che, C.; Wu, G.Q.; Qi, H.Y.; Huang, Z.; Yang, X.G. Uneven growth of thermally grown oxide and stress distribution in plasma-sprayed thermal barrier coatings. *Surf. Coat. Technol.* **2009**, *203*, 3088–3091. [CrossRef]

14. Song, J.; Qi, H.; Shi, D.; Yang, X.; Li, S. Effect of non-uniform growth of TGO layer on cracking behaviors in thermal barrier coatings: A numerical study. *Surf. Coat. Technol.* **2019**, *370*, 113–124. [CrossRef]

15. He, M.Y.; Evans, A.G.; Hutchinson, J.W. The ratcheting of compressed thermally grown thin films on ductile substrates. *Acta Mater.* **2000**, *48*, 2593–2601. [CrossRef]

16. Sun, Y.; Zhang, W.; Li, J.; Wang, T. Local stress around cap-like portions of anisotropically and nonuniformly grown oxide layer in thermal barrier coating system. *J. Mater. Sci.* **2013**, *48*, 5962–5982. [CrossRef]

17. Sun, Y.; Li, J.; Zhang, W.; Wang, T. Local stress evolution in thermal barrier coating system during isothermal growth of irregular oxide layer. *Surf. Coat. Technol.* **2013**, *216*, 237–250. [CrossRef]

18. Zhang, W.; Sun, Y.; Wang, T. Effect of spinel growth on the delamination of thermal barrier coatings. *Key Eng. Mater.* **2011**, *462*, 389–394. [CrossRef]

19. Suresh, S.; Giannakopoulos, A.E. A new method for estimating residual stresses by instrumented sharp indentation. *Acta Mater.* **1998**, *46*, 5755–5767. [CrossRef]

20. Zhao, X.; Xiao, P. Residual stresses in thermal barrier coatings measured by photoluminescence piezospectroscopy and indentation technique. *Surf. Coat. Technol.* **2006**, *201*, 1124–1131. [CrossRef]

21. Gelfi, M.; Bontempi, E.; Roberti, R.; Armelao, L.; Depero, L.E. Residual stress analysis of thin films and coatings through XRD experiments. *Thin Solid Films.* **2004**, *450*, 143–147. [CrossRef]

22. Tanaka, M.; Hasegawa, M.; Dericioglu, A.F.; Kagawa, Y. Measurement of residual stress in air plasma-sprayed Y_2O_3–ZrO_2 thermal barrier coating system using micro-Raman spectroscopy. *Mat. Sci. Eng. A.* **2006**, *419*, 262–268. [CrossRef]

23. Wu, R.T.; Wu, L.T. A powerful tool tomeasure residual stress in thermal barrier coatings: With the photoluminescence piezo-spectroscopy method, spallation life can be analytically predicted. *IEEE Nanotechnol. Mag.* **2017**, *11*, 20–23. [CrossRef]

24. Manero, A., II.; Selimov, A.; Fouliard, Q.; Knipe, K.; Wischek, J.; Meid, C.; Karlsson, A.M.; Bartsch, M.; Raghavan, S. Piezospectro-scopic evaluation and damage identification for thermal barrier coatings subjected to simulated engine environments. *Surf. Coat. Technol.* **2017**, *323*, 30–38. [CrossRef]

25. Lipkin, D.M.; Clarke, D.R. Measurement of the stress in oxide scales formed by oxidation of alumina-forming alloys. *Oxid. Met.* **1996**, *45*, 267–280. [CrossRef]

26. He, J.; Clarke, D.R. Determination of the piezospectroscopic coefficients for chromium-doped sapphire. *J. Am. Ceram. Soc.* **1995**, *78*, 1347–1353. [CrossRef]

27. Gong, X.Y.; Clarke, D.R. On the measurement of strain in coatings formed on a wrinkled elastic substrate. *Oxid. Met.* **1998**, *50*, 355–376. [CrossRef]

28. Munro, M. Evaluated material properties for a sintered alpha-alumina. *J. Am. Ceram. Soc.* **1997**, *80*, 1919–1928. [CrossRef]